SSRG International Journal of Electrical and Electronics Engineering
ISSN: 2348 – 8379 / https://doi.org/10.14445/23488379/IJEEE-V9I2P104

Volume 9 Issue 2, 28-36, February 2022

Original Article

Sub-Wavelength Electromagnetic Imaging Method Based on a Novel Low Loss Left-Handed Material

Jinyu Wang[1], Yaoliang Song[2]

[1]*Student, School of Electronic and Optical Engineering, NJUST, Nanjing, P.R.China*
[1] *Professor, School of Electronic and Optical Engineering, NJUST, Nanjing, P.R.China*

Received Date: 13 January 2022
Revised Date: 15 February 2022
Accepted Date: 27 February 2022

Abstract *- Negative refractive index materials have been proved to overcome the diffraction limit and realize sub-wavelength imaging, but the loss of materials will greatly limit the imaging quality. From the perspective of reducing loss, this paper designs a new left-handed (LH) material based on a nested split-ring resonator structure, which can be used for sub-wavelength imaging. The left-handed characteristic of this material is verified by effective constitutive parameter retrieval, and the loss characteristic is calculated by the figure of merit (FOM) coefficient. The transmission behaviours of propagating wave components and evanescent wave components in the lossy left-handed material during the imaging process are simulated, proving that the designed material can achieve very low loss left-handed characteristic around 9 GHz. As a result, the lens composed of a periodic arrangement of this left-handed structure can clearly distinguish two one-dimensional objects with sub-wavelength distance, thereby realizing super-resolution imaging around 9 GHz.*

Keywords — *Negative refractive index materials, Left-handed materials, Sub-wavelength imaging, Low loss, Evanescent waves.*

I. INTRODUCTION

The diffraction limit restricts the performance of traditional imaging systems, and the maximum resolution of these imaging systems can only reach $\lambda/2$, half of the incident wavelength. The reason for this phenomenon is that the detailed information of the imaging targets below $\lambda/2$ exists in the form of evanescent waves, which will decay exponentially after leaving the object's surface and cannot reach the imaging plane. This lost sub-wavelength information is the essential cause of the diffraction limit.

This work was supported in part by the National Natural Science Foundation of China (61271331, 61571229).

The diffraction limit theoretically determines the maximum resolution of a lens manufactured under optimal process conditions, which greatly limits the imaging quality. To overcome the diffraction limit and realize sub-wavelength imaging, Pendry proposed that metamaterial lenses with negative refractive index properties can effectively magnify the evanescent wave components in the imaging process [1], thereby providing a feasible way for sub-wavelength imaging. In 2005, the research team of Fang and Zhang used a 35nm silver film to make a superlens. The lens can perfectly reproduce the $\lambda/6$ sub-wavelength scale "NANO" image on the imaging plane at the wavelength of 365nm, which is the first superlens for subwavelength imaging [2]. In 2006, Thomas and Dmitriy used low-loss SiC replacing silver film and successfully achieved a resolution of $\lambda/20$ in the mid-infrared band [3]. These lenses use the plasma characteristics of some materials, such as silver, copper, SiC, et al. In a specific optical frequency band for imaging, but this is not suitable for microwave imaging because of the relatively lower frequency.

Left-handed materials, also called double-negative materials, are negative refractive index materials. Their main feature is that the effective permittivity and permeability are both negative, resulting in electric field vector E, magnetic field vector H, and wave vector k following the left-handed spiral orthogonality law in these materials. Left-handed materials do not exist in nature and can only be achieved by artificial design. The left-handed materials were firstly proposed by the former Soviet Union scientist Veselago in 1968 [4]. They were produced by the American scientist Smith in 2001 by combining periodic metal wire and split resonant ring (SRR) [5]. In recent years, researchers have designed many left-handed materials with different geometric structures, such as bifilar spiral structure [6], disc-shaped structure [7], multi-opening cross shape structure [8], and symmetrical "H"-shaped structure [9]. Unfortunately, these left-handed materials can exhibit relatively low loss characteristics in specific frequency bands, but the loss is not enough to realize sub-wavelength imaging. There are still

few reports on the practical application of left-handed structures for imaging. So far, overcoming the loss and realising sub-wavelength imaging in microwave bands using left-handed materials is still a research hotspot.

In this study, the sub-wavelength imaging characteristics of the left-handed materials in the presence of loss are considered. Firstly, a new left-handed material called nested split-ring resonator structure is designed. The effective constitutive parameters of this material are obtained by the simulated S-parameters and the improved retrieval algorithm of Kramers-Kronig relations. Then the left-handed characteristic and loss characteristic of the structure in the X-band can be concluded. After that, the transmission behaviours of propagation wave components and evanescent wave components in the metamaterial are simulated and analyzed. The result proves that the material can overcome the loss and transmit both components to a far region. Finally, the unit structure is periodically arranged into an imaging lens. The simulation result shows that the lens made of this metamaterial can achieve super-resolution imaging of two one-dimensional targets around 9GHz.

II. WAVE PROPAGATION IN LOSSY MATERIALS

According to the Abbe imaging theory, when a beam of electromagnetic wave with an angular frequency of ω incidents into a three-dimensional space, it is scattered after being irradiated on the object's surface. At this time, the electromagnetic wave carries the imaging information of the object, and this process is similar to modulation in communication systems. Suppose the propagation direction is along the $+z$ direction. In that case, the distribution of the field at any point in space can be regarded as the superposition of countless wavelets with transverse wave vector (k_x, k_y) and longitudinal wavenumber k_z, where $k_x^2 + k_y^2 + k_z^2 = k^2$. Some of these wavelets can reach the imaging plane, but others cannot. The more wavelets that can reach the imaging plane, the better the imaging quality. The electric field distribution can be Fourier expanded as

$$\boldsymbol{E}(x,y,z;t) = \int_{-\infty}^{+\infty}\int_{-\infty}^{+\infty} \boldsymbol{E}_\sigma(k_x,k_y)\times \exp(ik_x x + ik_y y + ik_z z - i\omega t)dk_x dk_y. \tag{1}$$

Since it is a time-harmonic field, the complex vector form of (1) can be obtained by Spatio-temporal separation

$$\dot{\boldsymbol{E}}(x,y,z) = \int_{-\infty}^{+\infty}\int_{-\infty}^{+\infty} \boldsymbol{E}_\sigma(k_x,k_y)\times \exp(ik_x x + ik_y y + ik_z z)dk_x dk_y. \tag{2}$$

Assuming that the incident electromagnetic wave is a P-polarized wave, that is, the direction of the electric field is always along the y axis direction, then the equation (2) can be simplified to

$$\begin{aligned}\dot{\boldsymbol{E}}(x,z) &= \int_{-\infty}^{+\infty}\int_{-\infty}^{+\infty} \boldsymbol{E}_\sigma(k_x)\exp(ik_x x)\exp(ik_z z)dk_x \\ &= \boldsymbol{E}_0(x)\exp(ik_z z),\end{aligned} \tag{3}$$

where:

$$\boldsymbol{E}_0(x) = \int_{-\infty}^{+\infty}\int_{-\infty}^{+\infty} \boldsymbol{E}_\sigma(k_x)\exp(ik_x x)dk_x. \tag{4}$$

The magnitude, sign, real part and imaginary part of the longitudinal wavenumber k_z all determine the propagation of the associated wavelet in the metamaterials, as described in (3). In the P-polarized wave,

$$k_z = \begin{cases} \pm\sqrt{k^2 - k_x^2}, & (k \ge k_x) \\ \pm i\sqrt{k_x^2 - k^2}. & (k < k_x) \end{cases} \tag{5}$$

When $k > k_x$, the longitudinal wavenumber k_z of the wavelet is real. There is only a phase change along the z-direction but no amplitude changes in the wavelet propagation. It is the propagating wave component in the electromagnetic wave; On the contrary, when $k < k_x$, the longitudinal wavenumber k_z is pure imaginary. At this time, the wavelet amplitude decays exponentially along the z-direction, but the phase does not change. The wavelet that owns a larger transverse wave vector is the evanescent wave component. It is the amplitude of the evanescent wave that decays sharply after leaving the object's surface that leads to the imaging resolution in the imaging system restricted to the diffraction limit of the wavelength order.

The loss of metamaterials is generally composed of three parts: substrate loss, ohmic loss and radiation loss [10]. The substrate loss can be measured by the loss tangent of the substrate material. In addition, studies have shown that the interaction between the substrate and different metal patterns will also affect the substrate loss; ohmic loss is the loss caused by the current flowing in the lossy metal and can be determined by the conductivity of the metal material; In the X-band, the radiation loss is small and can generally be ignored.

The performance of a negative refractive index material can be measured by the refractive index $n = n' + in''$, where the real part n' characterizes the refractive ability of the material, and the sign of n' can be used to judge whether the material is a positive refractive index material or a negative refractive index material at the current frequency; The imaginary part n'' is also called the loss coefficient, which represents the total transmission loss caused by the material, including the substrate loss and ohmic loss mentioned above.

To quantify the loss characteristic of materials at different frequencies, the concept of FOM (figure of merit) is introduced, which can be defined as

$$\mathrm{FOM}(\omega)=\left|\frac{n'(\omega)}{n''(\omega)}\right|. \tag{6}$$

For negative refractive index materials, the larger the FOM value, the better the negative refraction performance, the smaller the loss, and the better imaging effect can be obtained correspondingly.

Lossless negative refractive index materials have been proven to amplify evanescent waves, but lossless is only an ideal situation. Negative refractive index materials are often accompanied by greater loss, which will offset the evanescent wave's magnification by the material's negative refractive characteristics, making negative refractive materials often unable to achieve sub-wavelength imaging effects.

The wavenumber of the electromagnetic wave propagating in the material can be expressed by the vacuum wavenumber k_0 and the refractive index n,

$$k^2=k_0{}^2n^2=k_0{}^2(n'+in'')^2. \tag{7}$$

For P-polarized waves,

$$k_z{}^2=k^2-k_x{}^2=k_0{}^2(n'+in'')^2-k_x{}^2. \tag{8}$$

Let the longitudinal wavenumber $k_z=\beta_z+i\alpha_z$, in where β_z and α_z are called phase constant and amplitude constant along the z-axis, respectively. From (8), we easily have

$$\begin{cases}\beta_z{}^2-\alpha_z{}^2=k_0{}^2(n'^2-n''^2)-k_x{}^2\overset{def}{=}a_1,\\ 2\alpha_z\beta_z=2k_0{}^2n'n''\overset{def}{=}b_1.\end{cases} \tag{9}$$

Both β_z and α_z can be solved by (9) to obtain two sets of solutions opposite each other. Since the material used is lossy, the amplitude constant α_z must be greater than 0, $\beta_z>0$ in the right-handed medium, and $\beta_z<0$ in the left-handed material because the wave deflection direction is opposite to the energy transmission direction in the left-handed materials, so that the longitudinal wavenumber k_z can be expressed as:

$$k_z=\pm\sqrt{\frac{\sqrt{a_1{}^2+b_1{}^2}+a_1}{2}}+i\sqrt{\frac{\sqrt{a_1{}^2+b_1{}^2}-a_1}{2}}. \tag{10}$$

III. UNIT STRUCTURE DESIGN

For the realization of left-handed materials, many articles have discussed. At present, the most common method is to design left-handed materials concerning Smith's resonant structure, which can realize electrical resonance and magnetic resonance in the same frequency band so that the negative permittivity and negative permeability can be obtained at the same time to realize the left-handed characteristics [11-22].

Fig.1 shows the unit structure of the nested split-ring resonator structure designed in this paper. It can be approximated as a large split ring, with four small split rings nested inside, and these small rings are opposite each other.

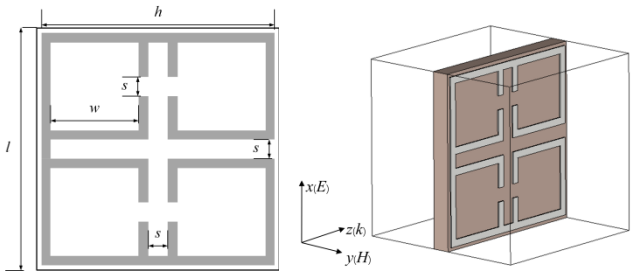

(a) Right view **(b) Overall view**

Fig. 1 The unit structure of designed left-handed material

Rogers RO3003 is used as the substrate layer material with a thickness of 0.25mm for its relatively small dielectric loss. The 0.017mm metal pattern is placed at one side of the substrate. Its material is copper with conductivity $\sigma = 5.96\times10^7(S/m)$. In addition, the value of parameters marked in Fig.1 is unit outside length $l = 2.5mm$, metal patch outside length $h = 2.4mm$, small rings inside length $w = 0.9mm$, the gap of the large and small rings $s = 0.2mm$. The 2.5mm length cube vacuum box is set, and $+z$ is the direction of the incident wave. The two waveguide walls perpendicular to the z-axis are respectively set as an input port (port1) and output port (port2), The two waveguide walls perpendicular to the x-axis are set as the ideal electric wall (PEC) of $E_t = 0$. The two waveguide walls perpendicular to the y axis are set as the ideal magnetic wall (PMC) of $H_t = 0$.

When designing the unit structure of the negative refraction index material for imaging, it is necessary to pay attention to the frequency band where the negative refraction characteristic is realized and minimize the material loss. The above structure uses the following methods to reduce the loss:

- Parallel incidence instead of vertical incidence. Parallel or vertical is relative to the substrate, as shown in Fig. 2(a). Vertical incidence means that the incident wave has greater contact with the metal patch, resulting in more loss caused by reflection and affecting imaging quality finally. So parallel incidence is suggested to use.

- Single-sided structure instead of double-sided structure. The double-sided structure was first proposed by Smith in 2001 (Fig. 2(b)). It has been widely adopted because it is easier to design. However, the electric resonance and magnetic resonance must pass through the substrate layer to be coupled, which will inevitably cause non-negligible substrate loss. Single-sided structure overcomes these problems by realizing electrical resonance and magnetic resonance on one side without passing through the substrate layer. Although the difficulty of unit design is increased, the loss can be effectively reduced.

- Double-negative instead of single-negative. The effective permittivity and effective permeability of the metamaterial can be expressed as $\varepsilon_r = \varepsilon' + i\varepsilon''$ and $\mu_r = \mu' + i\mu''$. Then the necessary and sufficient conditions for using metamaterial structure to achieve a negative refractive index are $\mu'\varepsilon'' + \mu''\varepsilon' < 0$ [23]. From the perspective of mathematical form, as long as the real and imaginary parts of the effective permittivity and the effective permeability are well controlled, both single-negative and double-negative materials can achieve a negative refractive index. However, single-negative materials tend to show greater loss when realizing negative refractive index because the imaginary part of effective permittivity or effective permeability is large inevitably. As a consequence, it is necessary to ensure that the frequency band for imaging is double-negative with negative effective permittivity and effective permeability when designing the metamaterial, that is, the left-handed material.

- Substrate material with a smaller loss. The loss tangent corresponds to the substrate loss in the metamaterial loss. We used Rogers RO3003 with relative permittivity of 3 and loss tangent of 0.001, instead of the more common FR-4 with relative permittivity of 4.3 and loss tangent of 0.025. Facts have proved that although the cost has increased, it is completely worth it.

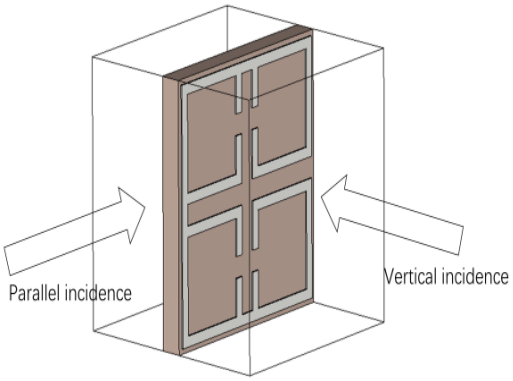

(a) Parallel incidence and vertical incidence

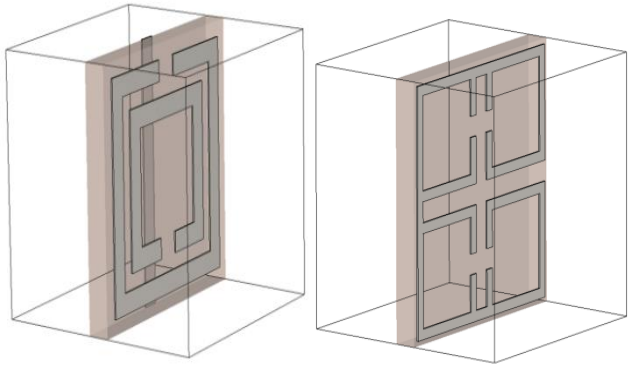

(b) Double-sided structure **(c) single-sided structure**

Fig. 2 Comparison of different incidence and structures

IV. LEFT-HANDED AND LOSS CHARACTERISTICS

A. Effective constitutive parameters retrieval

The amplitude and phase of S-parameters obtained by electromagnetic simulation software CST Microwave Studio 2017 are shown in Fig.4, and the simulated frequency range is set to 7GHz - 13GHz. It can be seen that there is an obvious transmission valley near 8.3GHz at Fig.4(a); At the same frequency, there is an abnormal mutation in the transmission phase as shown in Fig.4(b), which are all important features of negative refractive index materials, indicating that 8.3GHz is the dividing line of this designed metamaterial from positive refractive index material to negative refractive index material.

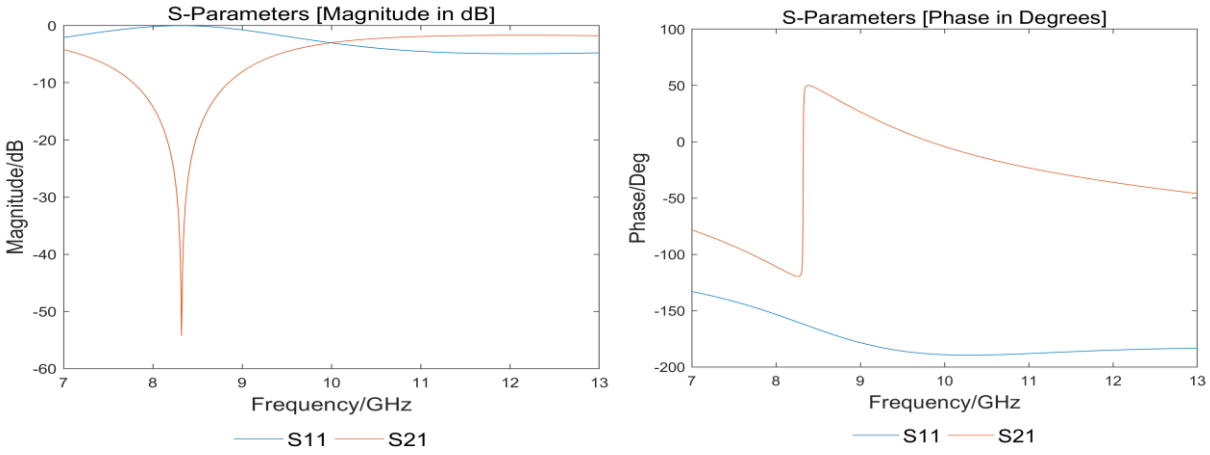

(a) Amplitude **(b) Phase**

Fig. 3 S-parameters of unit structure

Since the size of the unit structure is much smaller than the wavelength of the incident wave, metamaterials are regarded as molecular-scale materials, and its effective constitutive parameters such as relative impedance z, refractive index n as well as effective permittivity ε_r and effective permeability μ_r can be easily obtained by (11) - (14):

$$z = \pm\sqrt{\frac{(1+S_{11})^2 - S_{21}^{\ 2}}{(1-S_{11})^2 - S_{21}^{\ 2}}}, \tag{11}$$

$$n = \frac{1}{k_0 d}\arccos\left(\frac{1-S_{11}^{\ 2}+S_{21}^{\ 2}}{2S_{21}}\right), \tag{12}$$

$$\varepsilon_r = \frac{n}{z}, \tag{13}$$

$$\mu_r = n \cdot z, \tag{14}$$

where d is the effective thickness, namely thickness along the propagation direction.

In actual calculations, multi-value selection needs to be considered according to the physical meaning of parameters. In the calculation of the real part n' of the refractive index n, there will be a multi-branch problem. Here we use the Kramers-Kronig relationship improvement algorithm proposed by Ding Min [24,25] to solve it. The parameters of the unit structure are finally calculated as shown in Fig. 5:

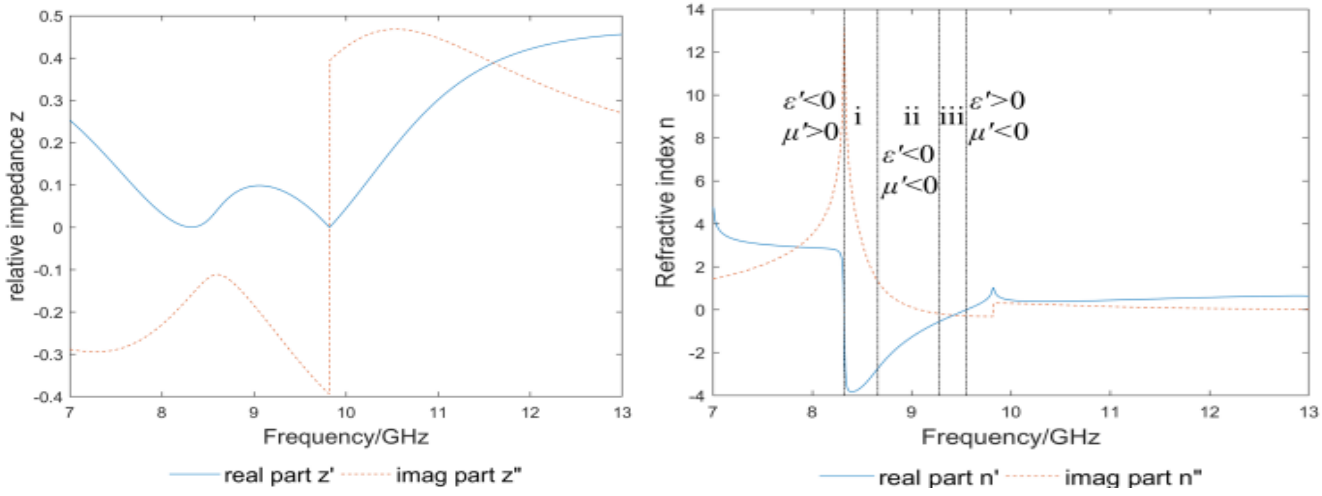

(a) Relative impedance z **(b) Refractive index n**

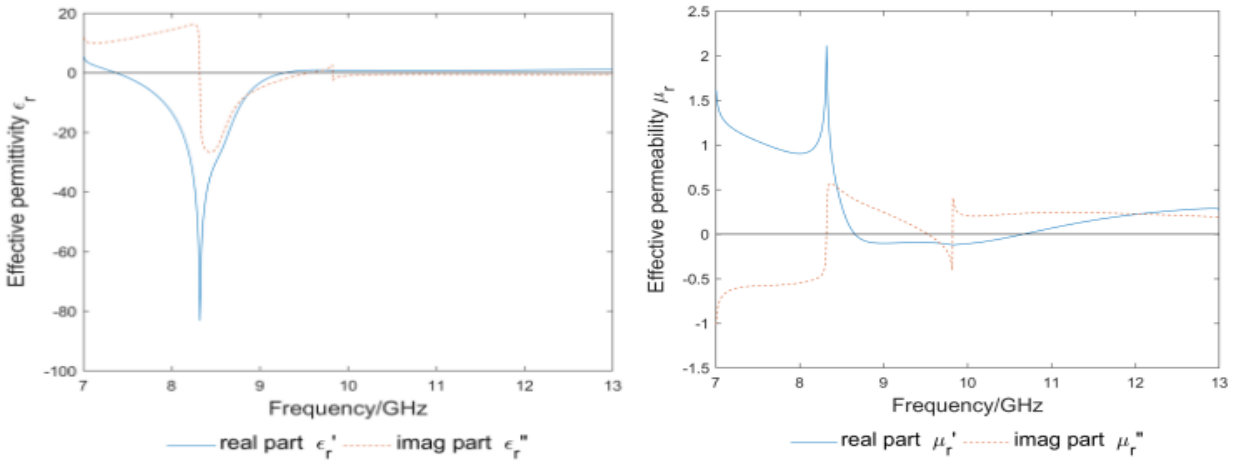

(c) Effective permittivity ε_r **(d) Effective permeability μ_r**

Fig. 4 The effective parameters of the unit structure

B. Left-handed characteristic

It is obvious from Fig. 4(b) that the real part of the refractive index changes from positive to negative around 8.3GHz, which is consistent with the analysis of S parameters in Fig.1, and then return to positive at 9.6GHz. Fig. 4(c) and 4(d) indicate that the effective permittivity and effective permeability of the designed metamaterial also show negative values in respective frequency bands, which are not exactly coincident with the negative refractive index bands. So, we have TABLE I:

Table 1. Frequency bands of negative parameters

	f_{min}/GHz	f_{max}/GHz
Negative refractive index	8.32	9.55
Negative permittivity	7.37	9.28
Negative permeability	8.66	10.67
Double-negative band	8.66	9.28

The designed metamaterial presents the negative refractive index by the type of double-negative at 8.66GHz - 9.28GHz, that is, the region(ii) in Fig. 4(b). On both sides of this frequency band, there also exist narrow negative refractive bands by the type of single-negative, where just effective permittivity or effective permeability is negative, the other one is positive, namely (i) and (iii) in Fig. 4(b). Although both single-negative and double-negative can achieve negative refractive, the imaginary part of refractive index n' that represents transmission loss is obviously smaller in the double-negative frequency band (ii) than single-negative frequency bands (i) and (iii).

C. Loss characteristic

The FOM value of the structure in the simulation frequency band has been calculated to measure the loss characteristic of the metamaterial, as shown in Fig. 5. It can be seen that the FOM value reaches the maximum around 9GHz, which is much higher than that at other frequencies, indicating that the loss of metamaterial reaches the minimum and theoretically has the ability of sub-wavelength imaging around 9GHz.

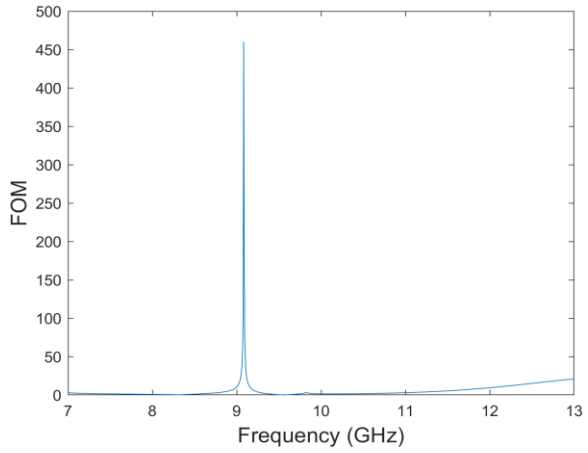

Fig. 5 FOM value of the left-handed material

V. IMAGING CAPABILITY ANALYSIS

At 9GHz, the refractive index of the designed metamaterial $n = -1.26 + i0.114$. The effective permittivity and effective permeability are both negative, and the loss is relatively small. In theory, it has sub-wavelength imaging ability. The transmission behaviour of the wave in the metamaterial has been simulated, and then the electric field distribution along the propagation direction of the wavelets with different transverse wavenumber k_x is obtained in Fig. 6.

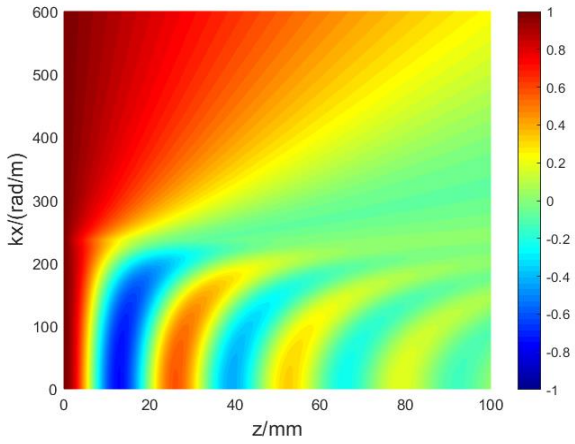

(a) 2-D amplitude

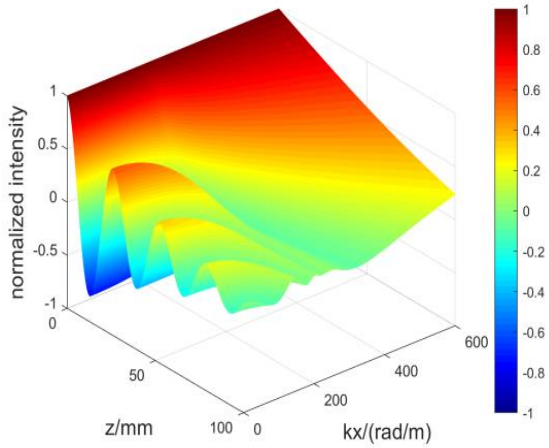

(b) 3-D amplitude

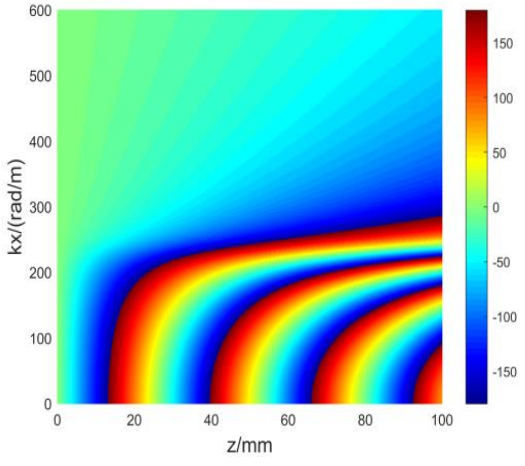

(c) Phase

Fig. 6 Electric field distribution of different transverse wavenumber at 9GHz

Different transverse wavenumber X correspond to different wave transmission modes: the wavelet with small k_x transmits in the form of propagation wave, and the amplitude is only affected by the loss of the material. When $k_x$is large enough, the wavelet transmits in the form of an evanescent wave. When the evanescent wave propagates in the left-handed material, its amplitude will be strengthened by the left-handed characteristic and attenuated by the loss characteristic simultaneously. As can be seen from Fig. 6, the decay of the evanescent waves is slow due to the small loss of the left-handed material. In this case, the evanescent wave components can be transmitted further along with the propagation wave components to achieve sub-wavelength imaging. As a contrast, the transmission of the wave has also been simulated at the lossless right-handed material of $n = 1$ and the lossy left-handed material at 8.5GHz of $n = -3.584 + i3.178$, respectively, as shown in Fig. 7.

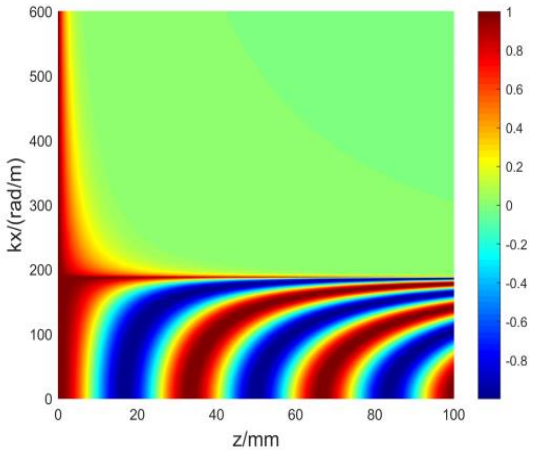

(a) n=1 lossless materials

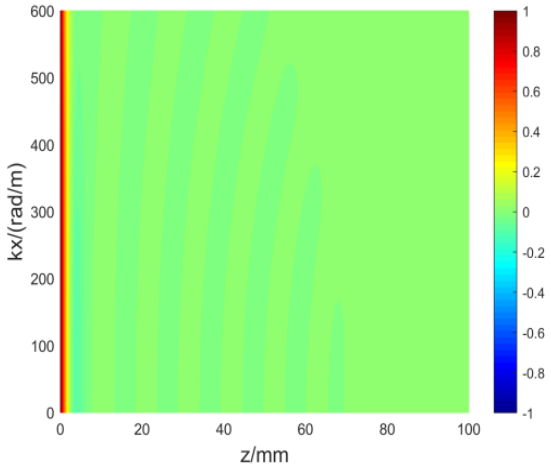

(b) Left-handed materials with large loss

Fig. 7 Electric field distribution in different materials

Fig. 7(a) proves that in lossless right-handed materials, the propagation wave components only change in phase, not in amplitude when the transmission, while the evanescent wave components decay rapidly in amplitude. Fig. 7(b) indicates that when the metamaterial loss is too large, neither the propagation wave components nor the evanescent wave components can be transmitted, and both of them will disappear inside the lossy material rapidly, resulting in the inability of the two components to participate in the imaging.

VI. LENS SIMULATION VERIFICATION

The unit metamaterial structure designed above is periodically arranged to make the lens for imaging, as shown in Fig. 8. Two discrete line sources that have a length of 20mm are set as targets requiring imaging and resolution. Compared with the 33mm wavelength of the wave at 9GHz, the distance between the two targets is 10 mm and belongs to the range of sub-wavelength. Two discrete line sources can independently radiate electromagnetic waves to free space and be placed 2mm in front of the lens.

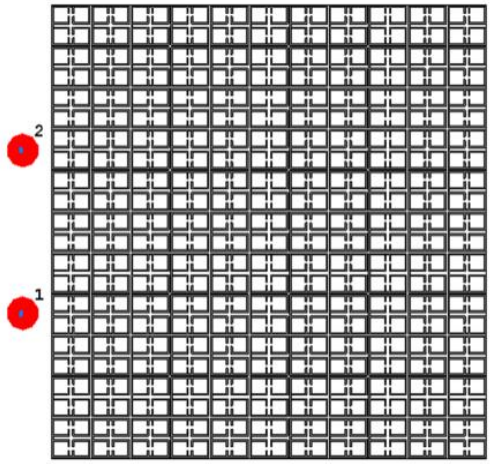

(a) Top view

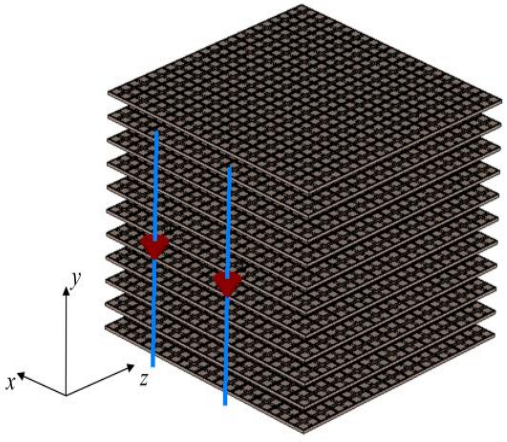

(b) Overall view

Fig. 8 The lens for imaging

The structure of Fig. 8 is simulated by CST, and the electric field distribution at 9 GHz is obtained, as shown in Fig. 9:

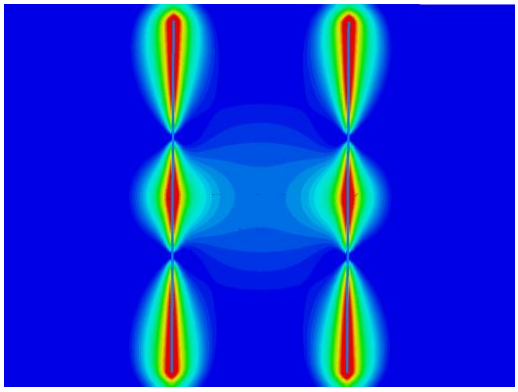

(a) Z-axis section (before the lens)

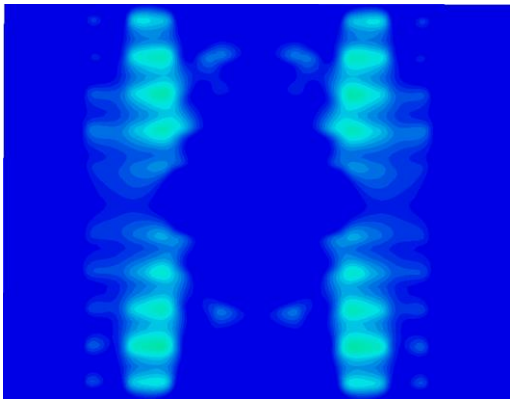

(b) Z-axis section (behind the lens)

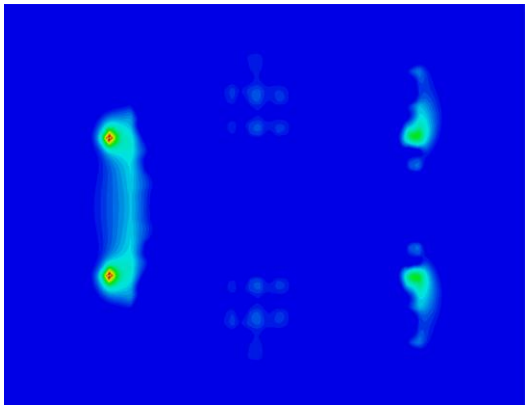

(c) Y-axis section

Fig. 9 The simulated electric field distribution

It is clearly in Fig. 9 that two one-dimensional targets with sub-wavelength distance can be clearly distinguished on the imaging plane behind the lens. Contrasting the electric field amplitude on the imaging plane before and after adding the lens, then Fig. 10 can be obtained.

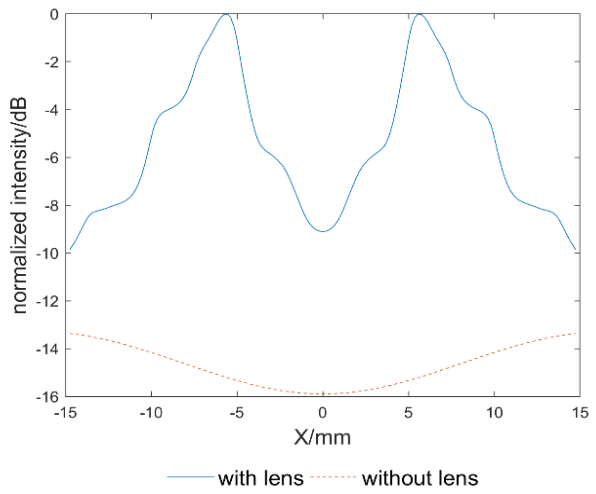

Fig. 10 Electric field amplitude before and after adding the lens

In Fig. 10, the dashed line represents the electric field distribution on the imaging plane without adding the lens, showing that the distinction between the two targets is very clear in this situation. After the lens is added, the solid line has been obtained, and two one-dimensional linear objects separated by 10mm can be clearly distinguished at the same position. There is a 10dB difference between the peak and the trough, so the lens made of designed left-handed material can achieve sub-wavelength imaging of two one-dimensional targets at 9 GHz.

VII. CONCLUSION

In order to overcome the diffraction limit, it is necessary to enhance the evanescent wave while minimizing the loss. Negative refractive index materials are proven to have the ability to amplify evanescent waves, but their losses are difficult to reduce. This paper summarizes several methods to effectively reduce loss and designs a novel left-handed material. The simulation shows that this material has both left-handed characteristics and low loss characteristics around 9GHz. When the electromagnetic wave propagates in this material, the attenuation speed of the evanescent wave components will slow down so as to obtain the ability to reach the imaging plane together with the propagation wave components. The lens composed of this structure can distinguish two targets with a distance of 10mm at 9GHz, demonstrating that this low loss left-handed material does have the ability of sub-wavelength imaging.

REFERENCES

[1] Pendry J B. Negative Refraction Makes a Perfect Lens[J]. Physical Review Letters, 85(18) (2000) 3966-3969.
[2] Fang N, Lee H, Cheng S, et al. Sub-Diffraction-Limited Optical Imaging with a Silver Superlens[J]. Science, 308(5721) (2005) 534-537.
[3] Taubner T, Korobkin D, Urzhumov Y, et al. Near-field microscopy through a SiC superlens.[J]. Science, 313(5793) (2016) 1595.
[4] Veselago, Viktor G. The Electrodynamics of Substances with Simultaneously Negative Values of Eandμ[J]. Physics-Uspekhi, 10(4) (1968) 509-514.
[5] D. R. Smith, W. J. Padilla, D. C. Vier, et al. Composite Medium With Simultaneously Negative Permeability and Permittivity [J]. Physical Review Letters, 84(18) (2000) 4184-4187.
[6] Juncheng L, Lixin G, Songhua L, et al. Design and Simulation of a Single-Sided Left-Handed Material in Thz Regimethz [J]. Acta Physica Sinica-Chinese Edition, 61(12) (2012) 124102-124102.
[7] Song Y C, Ding J, Guo C J, et al. Design and Analysis of a Broadband Metamaterial[J]. Journal of Microwaves, 31(2) (2015) 28-32.
[8] Wu L W, Zhang Z P. Broadband and Low-Loss Left-Handed Materials Based on Multi-Opening Cross Shape Structures[J]. Acta Physica Sinica -Chinese Edition, 65(16) (2016) 154101.
[9] Pan X, Minquan L I, Zhou Y, et al. Design and Analysis of Band and Low-loss LHM based on Symmetrical H-shape[J]. Journal of Materials Science and Engineering, 37(2) (2019) 223-227
[10] Wang J F, Qu S B, Xu Z, et al. A Method of Analyzing Transmission Losses in Left-Handed Metamaterials[J]. Chinese Physics Letters, 26(8) (2009) 4103.
[11] Akhter Z, Akhtar M J. Design of Unity Index Flat LHM Super-Resolution Lens for Near Field Millimetre-Wave Imaging Applications[C]//2014 IEEE Conference on Antenna Measurements & Applications (CAMA). IEEE, (2014) 1-4.
[12] Zhang X, Liu Z . Superlenses to Overcome the Diffraction Limit[J]. Nature Materials, 7(6) (2008) 435-441.
[13] Zhaowei Liu, Nicholas Fang, Ta-Jen Yen, and Xiang Zhang, Rapid Growth of Evanescent Wave by a Silver Superlens, Appl. Phys. Lett. 83(2003) 5184-5186.
[14] Durant S, Liu Z, Steele J M, et al. Theory of the transmission properties of an optical far-field superlens for imaging beyond the diffraction limit[J]. Journal of the Optical Society of America B, 23(11) (2006) 2383-2392.
[15] Liu Zhaowei, Durant Stéphane, Lee Hyesog, Pikus Yuri, Fang Nicolas, Xiong Yi, Sun Cheng, Zhang Xiang. Far-Field Optical Superlens.[J]. Nano letters,7(2)(2007).
[16] Liu Z, Lee H, Xiong Y, et al. Far-Field Optical Hyperlens Magnifying Sub-Diffraction-Limited Objects[J]. Science, 315(5819) (2007) 1686-1686.
[17] Lee, Hyesog, Liu, et al. Development of Optical Hyperlens for Imaging Below The Diffraction Limit[J]. Opt Express, (2007).
[18] Smith D R, Schultz S, Markos P, et al. Determination of Effective Permittivity and Permeability of Metamaterials from Reflection and Transmission Coefficients[J]. Phys. rev.b, 2001, 65(19):195104.
[19] Chen X, Grzegorczyk T M, Wu B I, et al. Robust Method to Retrieve the Effective Constitutive Parameters Of Metamaterials[J]. Physical Review E, 2004.
[20] Ya-Qiang Z, Guang-Ming W, Chen-Xin Z, et al. Design and Experimental Verification of Single-Layer High-Efficiency Transmissive Phase-Gradient Metasurface[J]. Acta Physica Sinica, 65(15) (2016).
[21] Smith D R, Mock J J, Starr A F, et al. Gradient Index Metamaterials[J]. Physical Review E, 71(3) (2005) 036609.
[22] Salami P, Yousefi L. Far-Field Subwavelength Imaging Using Phase Gradient Metasurfaces[J]. Journal of Lightwave Technology, 37(10) (2019) 2317-2323.
[23] Define R A, Lakhtakia A. A New Condition to Identify Isotropic Dielectric-Magnetic Materials Displaying Negative Phase Velocity[J]. Microwave and Optical Technology Letters, 41(4) (2004) 315-316.
[24] Peiponen E, Saarinen J J . Generalized Kramers-Kronig Relations in Nonlinear Optical- and THz-Spectroscopy.[J]. Reports on Progress in Physics, (2009).
[25] Min D, Hui X, Bo W, et al. The Comparisons Between Two Retrieve Algorithms for Metamaterials[J]. Acta Physica Sinica-Chinese Edition, 62(4) (2013) 44218-044218.